

**State-selective cross sections of multiple photoionization in Ne**

T. Kaneyasu, Y. Hikosaka, and E. Shigemasa

*UVSOR Facility, Institute for Molecular Science, Okazaki 444-8585, Japan*

F. Penent and P. Lablanquie

*LCP-MR, Université Pierre et Marie Curie-Paris 6 and CNRS (UMR 7614), 11 rue Pierre et Marie Curie, 75231 PARIS Cedex 05, France*

T. Aoto and K. Ito

*Photon Factory, Institute of Materials Structure Science, Oho, Tsukuba 305-0801, Japan*

(Received 25 April 2007; published 24 July 2007)

Valence double photoionization of Ne atom has been investigated by multielectron spectroscopy. Complete information on energy correlation between ejected electrons allows the identification of  $\text{Ne}^{2+}$  final states and their formation mechanism. In addition to simultaneous two-electron emission from the valence shells, indirect processes mediated by singly charged excited states have been observed. We have first obtained direct double-photoionization cross sections state-selectively in a wide photon energy region, by evaluating the contributions of the indirect processes. We have also applied the coincidence spectroscopy to three-electron emission from the valence shells. Even in the three-electron emission, the coincidence analysis enables to observe individual  $\text{Ne}^{3+}$  final states related to the triple-photoionization process and to obtain the state-selective cross sections.

DOI: [10.1103/PhysRevA.76.012717](https://doi.org/10.1103/PhysRevA.76.012717)

PACS number(s): 32.80.Fb, 32.80.Hd

**I. INTRODUCTION**

Double photoionization (DPI) of atoms and molecules caused by the absorption of a single photon is a fundamental process in atomic and molecular physics. Since the simultaneous ejection of two electrons cannot be described by the single-particle approximation, in which the photon interacts only with a single electron, the DPI process is entirely due to electron correlation. The study of DPI has long attracted considerable interest in both experimental and theoretical researches. So far numerous investigations of the DPI process have been concentrated on rare-gas atoms.

DPI leads to the production of doubly charged ions. Ion mass spectrometry has been extensively used for investigating the DPI process, where the total DPI cross section or the ratio of double to single ionization is determined from the ion yield curves measured as a function of photon energy [1]. Particularly in He atoms, direct DPI—i.e., simultaneous two-electron emission—can directly be accessed from the mass-resolved ion yields [2], since only the  $\text{He}^{2+}$  ( $^1S$ ) final state is produced through DPI and indirect (or sequential) processes via singly charged excited states cannot contribute to the DPI cross section. In contrast, valence DPI of the other rare gases leads to the formation of various states and the presence of indirect processes should be considered [3]. The mass spectrometry has been used to investigate DPI cross sections of the rare gases heavier than He in early studies [4–8], but gives only the total DPI cross section. In theoretical works, DPI cross sections have been calculated for direct two-electron emission, leading to specific doubly charged states [9–12], and thus it is required to observe direct DPI state-selectively.

Meanwhile, state-selective DPI cross sections can be identified by fluorescence spectroscopy in the case where the doubly charged states further decay via fluorescence emis-

sion. In practice state-selective DPI cross sections have been obtained for processes leading to  $ns^0np^4$  and  $ns^1np^5$  states of Ne and Ar using fluorescence spectroscopy [13,14], though indirect DPI processes were included in the results obtained.

Direct DPI produces two electrons with a continuous energy distribution from zero to the maximum available energy, which is generally difficult to observe in the usual photoelectron spectroscopy. Photoelectron spectroscopy based on the time-of-flight method has been successfully used for observing both the direct and indirect DPI processes of rare gases [15], since this method allows keeping a transmission function almost constant in a wide kinetic energy region. The continuum distribution of emitted electrons due to the direct DPI process and its shape changing with photon energy have been clearly observed for He atoms with a single double-ionization continuum [16]. However, for all heavier rare-gas atoms, it is impossibly difficult to separate the various DPI continua by conventional photoelectron spectroscopy, since a large portion of them overlap each other and even the steps corresponding to the different DPI final states are invisible in the experimental spectra. Electron-electron coincidence spectroscopy, which allows analysis of the energy of ejected electrons through the DPI process, is indispensable for addressing a wide variety of the DPI cross sections.

In this work, we have investigated valence DPI of Ne by multielectron spectroscopy [17]. By using a magnetic-bottle electron time-of-flight (TOF) spectrometer, all electrons ejected in every multiple-photoionization event are analyzed in energy. The coincidence data sets thus obtained give complete information on the energy correlation between ejected electrons. The cross sections of direct DPI leading to the formation of the  $2s^22p^4(^3P, ^1D, ^1S)$ ,  $2s^12p^5(^3P, ^1P)$ ,  $2s^02p^6(^1S)$ , and satellite  $\text{Ne}^{2+}$  states have been measured in a photon energy region from 69.89 eV to 239.8 eV, and are compared with theoretical state-selective DPI cross sections

of Ne calculated by using a nonvanishing lowest-order perturbation theory [11,12]. Additionally, the coincidence data sets, which are obtained above the triple-photoionization (TPI) thresholds, contain information on three-electron emission from valence shells. We have also derived the valence TPI cross sections of Ne. It is nicely demonstrated that the coincidence electron spectroscopy makes it possible to observe the three-electron emission and to separate  $\text{Ne}^{3+}$  states related to the TPI process.

## II. EXPERIMENT

The experiments were carried out on the beamlines of BL-1C [18] and BL-16B [19] at the Photon Factory in Tsukuba, Japan. During the measurements, the storage ring was operated in the single-bunch mode, providing a 624-ns period between light pulses. The photon energy resolution ( $E/\Delta E$ ) was set to about 3000, and the absolute photon energy was calibrated with total electron-yield measurements on the resonances of rare-gas atoms.

The multicoincidences were recorded for electrons which were analyzed in energy by their TOF in a magnetic-bottle electron spectrometer. The apparatus and the data acquisition scheme has been described briefly elsewhere [20,21]. The monochromatized photon beam crossed at right angle an effusive gas beam from a needle with the inside diameter 500  $\mu\text{m}$ . Electrons ejected from sample gases after interaction with the photons are guided in a 2.5-m flight tube by the strong magnetic field of a 7000-G permanent magnet, whose top was located at several mm from the interaction region. The magnetic field inside the flight tube was kept at 10–20 G to conduct the electrons to a detector of two microchannel plates (MCPs). The flight tube was surrounded by a 1-mm-thick  $\mu$ -metal tube to be shielded magnetically against Earth's magnetic field. The electron signals from the detector were fed into a time-to-digital converter (RoentDek TDC-8PCI) as a start signal, while a ring clock was used as a stop signal. The signal of the fastest electron among multiple electrons produced in a photoabsorption event was used to trigger the TDC. The electron kinetic energies were calibrated using the He 1s photoelectron lines at known photon energies. The energy resolution for the TOF analyzer was constant at  $E/\Delta E \sim 50$  below 200 eV kinetic energy. From the comparison between electron yields and photoion yields of He, we have found that the detection efficiency was almost constant below 200 eV kinetic energy and gradually decreased with increasing kinetic energy. In the present work the detection efficiency was estimated by comparing the ratio between the total DPI yield and the sum of single 2s and 2p photoionization yields of Ne with those in the literature [22]. The efficiency thus obtained was  $59\% \pm 9\%$ , which corresponds to the MCP detection efficiency, in the whole photon energy region.

## III. RESULTS AND DISCUSSION

### A. Double photoionization

#### 1. DPI branching ratio

Figure 1(a) shows an example of kinetic energy correlation maps between the fast and slow electrons associated

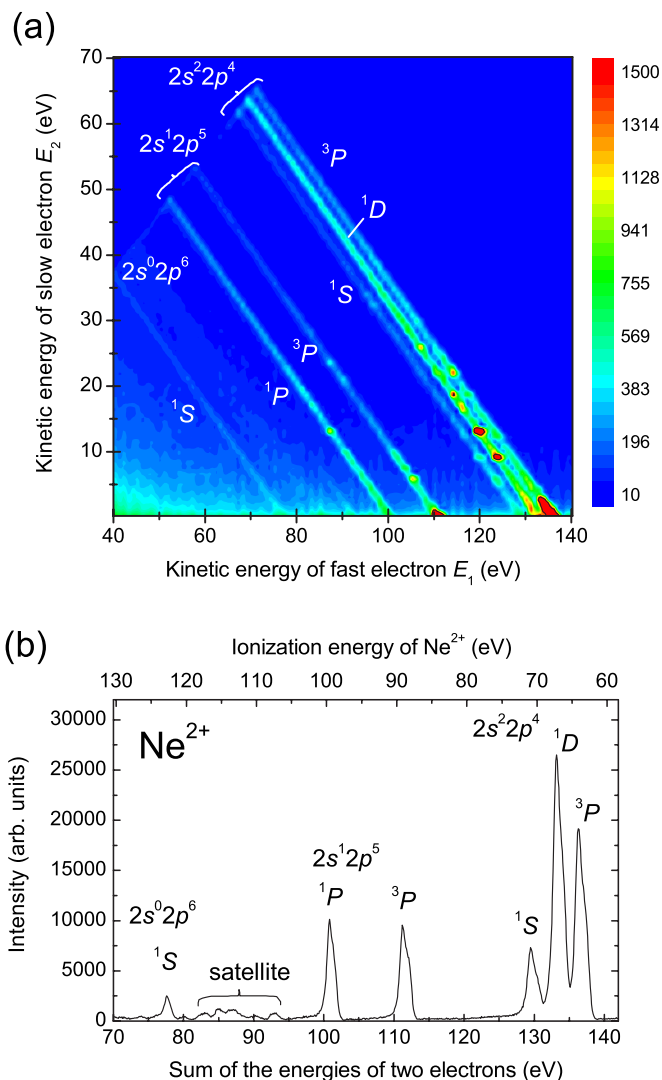


FIG. 1. (Color online) (a) Two-dimensional map for kinetic energy correlation of two-electron coincidence pairs in Ne DPI at  $h\nu=200.4$  eV. Accumulation time was 6 h. The DPI intensity is plotted in linear scale. The two-dimensional map is discretized with 0.5 eV and 0.4 eV steps for fast and slow electrons, respectively. (b) Histogram of the kinetic energy sum of the two electrons extracted from the two-dimensional map in (a). Discretization by 0.1 eV step is adopted for the histogram.

with valence DPI of Ne, which was measured at  $h\nu=200.4$  eV. The excess energy, which corresponds to the energy difference between the photon energy and the DPI ionization energy for each  $\text{Ne}^{2+}$  state, can be continuously shared between the two electrons, and hence the diagonal lines on the two-dimensional (2D) map correspond to formation of the final  $2s^2 2p^4(^3P, ^1D, ^1S)$ ,  $2s^1 2p^5(^3P, ^1P)$ , and  $2s^0 2p^6(^1S)$  states. To reveal the final  $\text{Ne}^{2+}$  states produced through DPI, a histogram of the kinetic energy sum for two electrons is constructed by summing the coincidence counts on the 2D map along the diagonal lines. The energy-sum spectrum in Fig. 1(b) is plotted as a function of the  $\text{Ne}^{2+}$  ionization energy and of the kinetic energy. Similar analyses have been performed for the 2D maps measured at different photon energies. Relative contributions of the individual

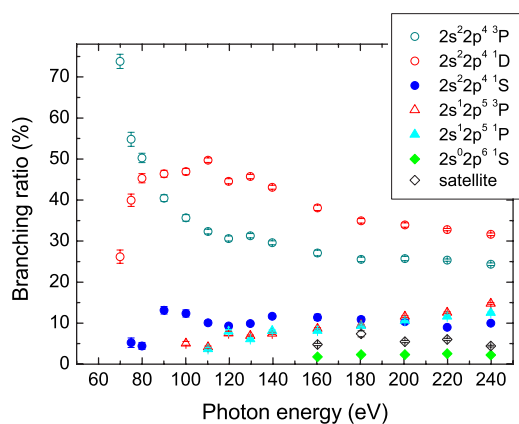


FIG. 2. (Color online) DPI branching ratios derived from the energy-sum spectrum of the two electrons.

$\text{Ne}^{2+}$  states and weak satellite states to the total DPI yields are determined from the corresponding peaks using a least-squares fitting with Gaussian functions. The shapes of the peaks in the energy-sum spectrum are somewhat asymmetric, and tails to the low-kinetic-energy sides are seen. It is likely that such peak shapes are due to the property of the present spectrometer.

DPI branching ratios derived from the energy-sum spectra are shown in Fig. 2 as a function of the photon energies. The DPI branching ratio shows remarkable photon energy dependence and differs significantly from that deduced from the statistical weights. For instance, the intensity ratio of the  $2s^2 2p^4 ({}^3P, {}^1D)$  states compared to the  $2s^2 2p^4 ({}^1S)$  state is 10:7.6:1 at 74.92 eV, while this drastically changes to 2.4:3.2:1 at 239.8 eV. Such behavior is reflected in the contribution of the indirect DPI and concerned with the electron-electron correlation as was explained in terms of inelastic internal collision (knockout or two-step one) [8–10,23] where an electron created after absorption of a photon knocks the other electron out of an atom in a second step of the collision. The inelastic collision mainly contributes to DPI cross section in a lower-photon-energy region because the slow primary electron has sufficient time to interact with other electrons [23]. The DPI branching ratio may deviate from the statistical weights due to the existence of the inelastic collision, whose contribution differs with each DPI final state depending on the excess energy.

The relative intensities of the final states derived from the energy-sum spectrum are the sum of direct and indirect DPI yields. The indirect processes are obviously seen as enhanced spots in the 0–40 eV range of slow electrons on the 2D map in Fig. 1(a). To clarify the presence of the indirect DPI, slow electron energy spectra are obtained by projecting the 2D map onto the vertical axis. Figure 3 shows the slow electron spectra associated with the formation of the  $2s^2 2p^4 ({}^3P)$ ,  $2s^2 2p^5 ({}^3P)$ , and  $2s^0 2p^6 ({}^1S)$  states. It should be noted that false coincidences considerably affect the slow electron spectra in the kinetic energy region close to 0 eV. The slow electron spectra result from false coincidences were deduced from the 2D map in Fig. 1(a), by considering a certain region close to the diagonal line corresponding to the formation of each  $\text{Ne}^{2+}$  final state. For instance, the slow

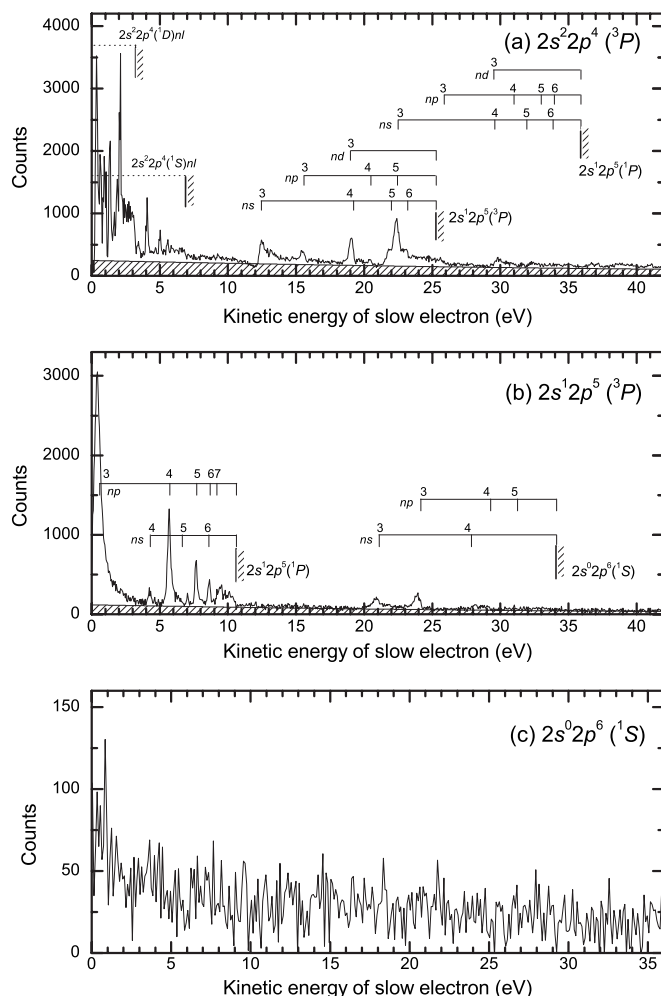


FIG. 3. Slow electron energy spectra in the DPI of Ne leading to (a)  $2s^2 2p^4 ({}^3P)$ , (b)  $2s^2 2p^5 ({}^3P)$ , and (c)  $2s^0 2p^6 ({}^1S)$  states measured at  $h\nu=200.4$  eV. The shaded areas represent the contributions of the direct DPI. The intermediate singly charged Rydberg states related to the indirect DPI processes are indicated in the figures. Discretization by 50 meV step is adopted for the histograms.

electron spectrum associated with the formation of the  $2s^2 2p^4 ({}^3P)$  state was derived from the diagonal line [corresponding to the 135–138.9 eV range in Fig. 1(b)] on the 2D map, while the false coincidence spectrum was deduced for a vicinal area [corresponding to the 138.9–140.4 eV range in Fig. 1(b)]. In the present analyses, the net electron spectra have been obtained by subtracting such contributions from the raw spectra. Simultaneous two-electron emission results in a U-shaped electron energy distribution [4]. One can expect that peak structures are superimposed on the U-shaped energy spectrum, when the indirect DPI occurs in addition to the direct processes. The contribution of the indirect DPI is obvious when the two-electron emission leads to the  $2s^2 2p^4 ({}^3P, {}^1D, {}^1S)$  and  $2s^2 2p^5 ({}^3P, {}^1P)$  final states, as demonstrated in Figs. 3(a) and 3(b). The intermediate excited states associated with the indirect DPI are indicated on the energy spectra, and the assignments are made with spectroscopic data obtained by threshold photoelectron spectroscopy [24], photoelectron spectroscopy [25], and second-step Auger

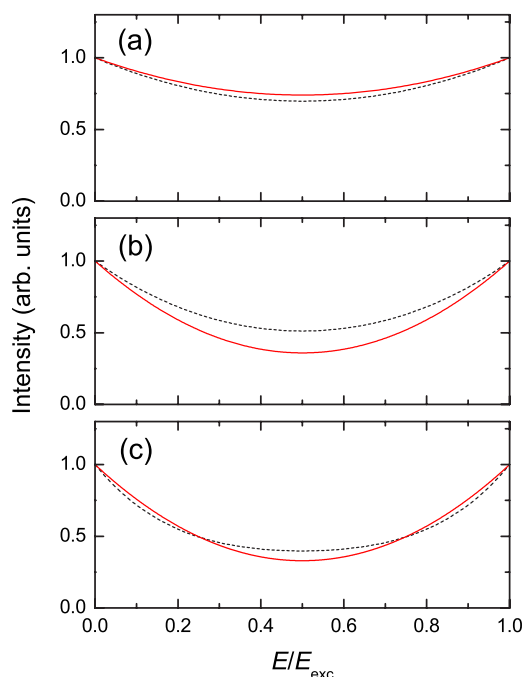


FIG. 4. (Color online) Calculated photoelectron spectra (dotted line) [9] and the hyperbolic curves (solid line) used to estimate the direct DPI intensity into the  $2s^2 2p^4$  ( $^3P$ ) state. The horizontal axis corresponds to the kinetic energy  $E$  normalized to the excess energy  $E_{\text{exc}}$ . The curves were calculated for excess energies of (a) 20, (b) 45, and (c) 90 eV. The excess energies in the present measurement are (a) 17.7, (b) 47.8, and (c) 97.9 eV.

electron spectroscopy following the core excitation into Rydberg states [26]. More detailed analysis on the indirect DPI will be given in a forthcoming paper. Conversely, the slow electron spectrum in the  $2s^0 2p^6$  ( $^1S$ ) state shows the U-shaped energy distribution and no peaked structures due to the indirect processes [see Fig. 3(c)]. No significant peak structures are detected on the slow electron spectra associated with the formation of the satellite states (not shown in figures), similar to the case of the DPI leading to the  $2s^0 2p^6$  ( $^1S$ ) state. Therefore, it is conjectured that these states result mainly from simultaneous two-electron emission in the photon energy region of interest.

To obtain the direct DPI cross section, we need to evaluate its relative intensity compared to the sum of the direct and the indirect DPI cross sections. The ratio between the direct and indirect processes is determined for the DPI into the  $2s^2 2p^4$  ( $^3P$ ,  $^1D$ ,  $^1S$ ) and  $2s^1 2p^5$  ( $^3P$ ,  $^1P$ ) states, assuming that the direct DPI contribution can be expressed by hyperbolic curves [shaded areas in Figs. 3(a) and 3(b)] and neglecting interference effect between the discrete singly charged states and the DPI continua. In Fig. 4, the obtained hyperbolic curves for the contribution of direct DPI into the  $2s^2 2p^4$  ( $^3P$ ) state are compared with the theoretical curves calculated by many-body perturbation theory [9]. The theoretical electron spectra were calculated for two-electron emission from the  $2p$  subshell with excess energies of 20, 45, and 90 eV, whereas experimental curves are gained for slightly lower or higher excess energies of 17.7, 47.8, and 97.9 eV. The kinetic energy scales in the electron spectra are

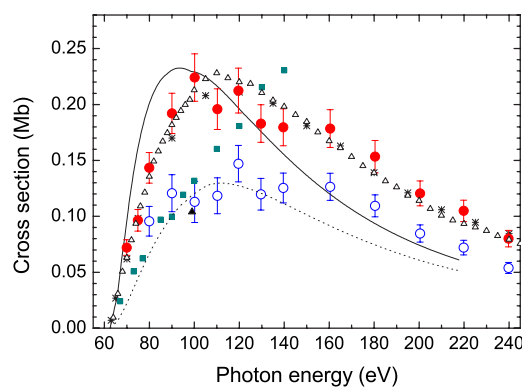


FIG. 5. (Color online) Total DPI cross sections of Ne as a function of photon energy in comparison with other experimental and theoretical data. Experiment: ●, present work for the sum of direct and indirect DPI; ○, present work for the direct DPI; \*, Ref. [6]; Δ, Ref. [22]; ■, Ref. [27]; ▲, Ref. [28]. Theory: dotted and solid lines are obtained in length and velocity form, respectively, in Ref. [11]. Note that all the theoretical curves of Refs. [11,12] shown in figures have been obtained by using the  $V^{(N-2)}$  potential.

normalized to the excess energies. The hyperbolic curves largely reproduce the calculated spectra, and therefore a reasonable estimation can be made for the direct DPI contribution in the slow electron spectra. Although the above assumption may be rough, it is expected that the accuracy of the estimated ratio between the direct and indirect processes is within 20%.

## 2. Total DPI cross sections

The absolute total DPI cross sections are derived by normalizing the sum of the  $2s$  and  $2p$  single photoionization yields with those in the literature [22] at each photon energy. The absolute total DPI cross sections thus obtained are presented in Fig. 5 with other experimental data and theoretical curves. The total DPI cross section, corresponding to the sum of the direct and indirect processes for the all final  $\text{Ne}^{2+}$  states, is depicted by solid circles, whereas the open circles represent the total direct DPI cross section. The theoretical curves are obtained by Kilin *et al.* [11,12] in the dipole length and velocity forms. The experimental cross sections in the literature [6,22] include the contribution of the indirect DPI as the present investigation reveals. Meanwhile, direct DPI cross sections were obtained by photoelectron spectroscopy based on the TOF method [27] and by triple-differential cross-section measurements [28]. The agreement between our result on the sum of the direct and indirect processes with the experimental results obtained by photoion mass spectrometry validates our procedure to derive the absolute values from the relative yields. The direct DPI cross sections roughly agree with the ones reported by Becker and Wehlitz [27] from the threshold to 100 eV, whose results, however, exhibit monotonically increasing behavior with increasing photon energy. In conventional photoelectron spectroscopy, it is hard to separate the DPI continua and to estimate the direct DPI yields from the photoelectron spectra. This is the most probable reason for such a large deviation between the experimental result by Becker and Wehlitz and ours. In the

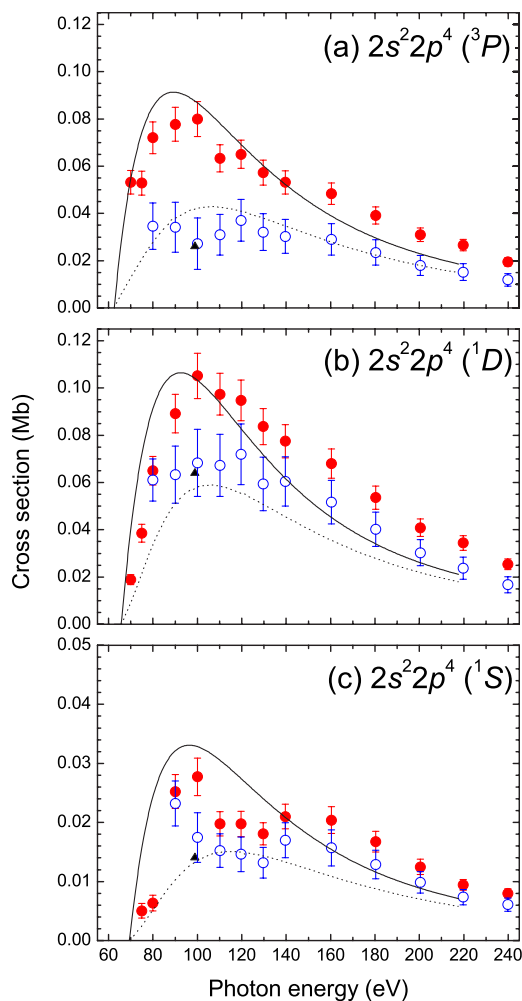


FIG. 6. (Color online) State-selective DPI cross sections of Ne leading to formation of  $2s^2 2p^4$  (a)  $^3P$ , (b)  $^1D$ , and (c)  $^1S$  states as a function of photon energy in comparison with theoretical data. Experiment: ●, present work for the sum of direct and indirect DPI; ○, present work for the direct DPI; ▲, Ref. [28]. Theory: dotted and solid lines are obtained in length and velocity form, respectively, in Refs. [11,12].

theoretical work, indirect DPI has not been taken into account and thus the direct DPI cross-section measurement should be used for comparison with the theoretical curve. In the low-energy region, from threshold to 140 eV, the length-form cross section reproduces direct DPI, while the velocity-form cross sections show better agreement with our results at higher photon energy.

### 3. State-selective DPI cross sections

The partial cross sections for individual final states are obtained from the relative DPI intensities of the final  $\text{Ne}^{2+}$  states and total DPI cross sections. Here, using the ratio between the direct and indirect processes, which is estimated from the slow electron spectra, direct DPI cross sections are also obtained for each final state. The state-selective DPI cross sections for the  $2s^2 2p^4(^3P, ^1D, ^1S)$  states thus obtained are shown in Fig. 6. Scherer *et al.* [28] obtained absolute cross sections on direct DPI leading to these final states

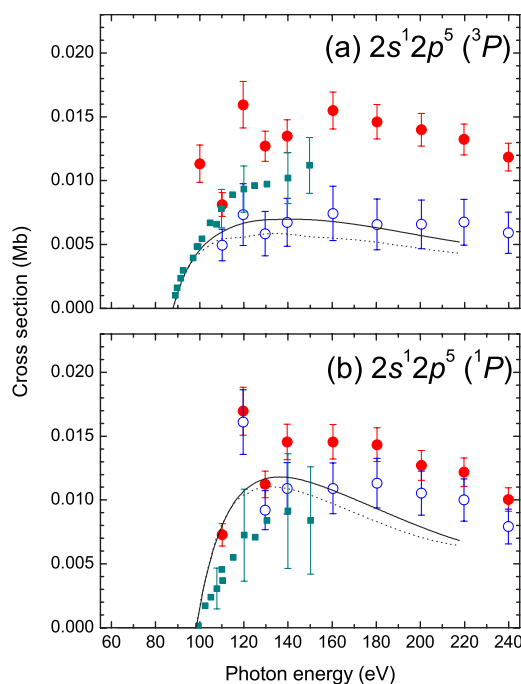


FIG. 7. (Color online) State-selective DPI cross sections of Ne leading to  $2s^1 2p^5$  (a)  $^3P$  and (b)  $^1P$  states as a function of photon energy in comparison with theoretical data. Experiment: ●, present work for the sum of direct and indirect DPI; ○, present work for the direct DPI; ■, Ref. [13]. Theory: dotted and solid lines are obtained in length and velocity form, respectively, in Ref. [11].

through a normalization of their triple-differential cross sections to He data. The obtained cross sections are available only at the photon energy of 99 eV, as depicted by triangles in Fig. 6, and their results show good agreement with the present result. The present data set is the first case for evaluating the theoretical results in a photon energy ranging from the DPI thresholds to 239.8 eV. In the lower-photon-energy side, it is rather difficult to estimate the relative intensity of the direct process and the direct DPI cross sections are not obtained at photon energies less than 75 eV and 80 eV for the  $2s^2 2p^4(^3P, ^1D)$  and  $2s^2 2p^4(^1S)$  states, respectively. The direct DPI cross sections for each state roughly follow the theoretical curve calculated in the length-form.

In Fig. 7, the DPI cross sections for the  $2s^1 2p^5(^3P, ^1P)$  states are compared with the experimental results obtained by fluorescence spectroscopy [13] and the theoretical curves. The fluorescence cross sections include both direct and indirect processes as mentioned above. The DPI cross sections obtained by fluorescence spectroscopy exhibit slightly lower values than our results on the sum of the direct and indirect processes. For the  $^3P$  state, the experimental results on the direct process fairly agree with the theoretical velocity-form curve above 110 eV. In the  $^1P$  state, a general tendency of the present results, neglecting the data point at 120 eV, resembles the theoretical curves in shape.

Concerning the DPI process leading to the  $2s^0 2p^6(^1S)$  state and the satellite states, their cross sections are one or two orders of magnitude lower than the other DPI processes. The corresponding DPI cross sections are presented in Fig. 8 with the cross sections deduced by the fluorescence measure-

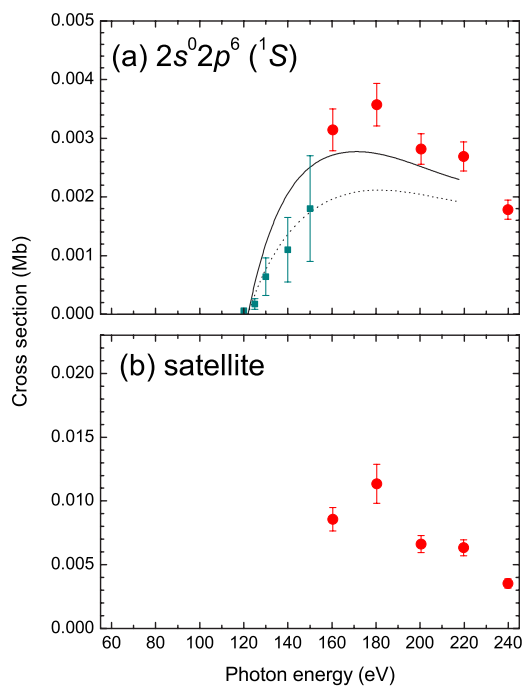


FIG. 8. (Color online) State-selective DPI cross sections of Ne leading to (a)  $2s^0 2p^6 ({}^1S)$  and (b) satellite states as a function of photon energy in comparison with theoretical data. Experiment: ●, present work for the sum of direct and indirect DPI; ■, Ref. [13]. Theory: dotted and solid lines are obtained in length and velocity form, respectively, in Ref. [11].

ment and theoretical calculation. As demonstrated in the slow electron spectra shown in Fig. 3(c), no indirect process can be found for these states. For the cross sections of the  $2s^0 2p^6 ({}^1S)$  state, the velocity-form cross sections show better agreement with our results obtained above 160 eV, while the fluorescence cross sections show remarkable agreement with the length-from cross section in the energy region from the threshold to 150 eV. The cross sections of DPI leading to the satellite states are displayed in Fig. 8(b). The satellite DPI contributes to almost 5% of the total DPI cross sections from 160 eV to 240 eV. It will be needed to take account of the satellite transitions, to deduce DPI amplitude theoretically in the higher-photon-energy side. However, such contributions have not been considered in any theoretical studies so far.

### B. Triple photoionization

Previous experimental investigations of the TPI of Ne have been limited to cross-section measurements by using mass spectrometry. While detailed cross-section measurements have been made near the TPI threshold to observe the threshold law [29,30], only a study reported on the TPI cross sections in a wide photon energy range [7]. We have deduced the coincidence for three-electron emission from the valence shells to obtain TPI cross sections. In Fig. 9(a), we present a histogram for the sum of the kinetic energies of three correlated electrons at  $h\nu=239.8$  eV. Comparing with the previous spectroscopic data [31,32], the three peaks in the sum spectrum can be assigned to  $2s^2 2p^3 ({}^4S, {}^2D, {}^2P)$  final  $\text{Ne}^{3+}$

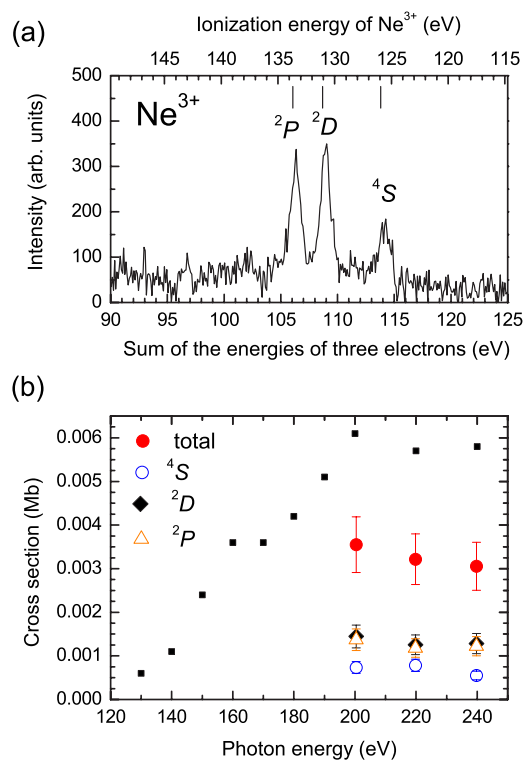


FIG. 9. (Color online) (a) Sum of energies of three correlated electrons at  $h\nu=239.8$  eV. The vertical bars indicate energy levels of the  $\text{Ne}^{3+}$  states, which are derived from the relative energies of the  $\text{Ne}^{3+}$  states [31] and the TPI threshold [32]. Discretization by 0.1 eV step is adopted for the histogram. (b) Total and state-selective TPI cross sections. Previously reported total cross sections [7] are plotted as ■.

states. Following the same normalization procedure as applied to the DPI, state-selective TPI cross sections can be deduced. Figure 9(b) shows the corresponding cross sections. The total TPI cross section is two orders of magnitude lower than that of DPI. The total TPI cross sections obtained in the present work are about half of those determined by photoion spectroscopy [7]. This difference may be originated from the insufficient signal-to-noise ratio in the previous measurements, since the TPI cross sections are considerably small. Although no information on the formation mechanism of  $\text{Ne}^{3+}$  states has been given in the present study, it is expected that the TPI process is caused not only by direct three-electron emission but also by indirect processes. The coincidence spectroscopy potentially allows us to investigate such indirect processes and to identify the formation mechanism of triply charged states.

### IV. SUMMARY

Two-electron emission from valence shells of Ne, which leads to formation of several doubly charged final states, has been investigated using multielectron spectroscopy. The  $\text{Ne}^{2+}$  final states and their relative yields are well identified from the coincidence data sets. For DPI into the  $2s^2 2p^4 ({}^3P, {}^1D, {}^1S)$  and  $2s^1 2p^5 ({}^3P, {}^1P)$  states, the indirect processes mediated by the excited states of the singly

charged ions are found in the slow electron spectra. We have firstly obtained the direct DPI cross sections state-selectively in a wide photon energy range by considering the presence of the indirect DPI. The observation of direct DPI allows one to evaluate theoretical models for describing two-electron emission from a many-electron atom. This has been achieved by utilizing the complete information on the energy correlation among the ejected electrons. The direct DPI cross sections are compared with those calculated by the nonvanishing lowest-order perturbation theory. The length-form cross sections roughly reproduce the direct DPI cross sections for the  $2s^2 2p^4(^3P, ^1D, ^1S)$  states. For direct DPI into the  $2s^1 2p^5(^3P, ^1P)$  and  $2s^0 2p^6(^1S)$  states, the velocity-form cross sections show a better agreement with our results. Additionally, the coincidence spectroscopy has been applied to inves-

tigate the valence TPI of Ne. The energy-sum spectrum of three correlated electrons reveals  $\text{Ne}^{3+}$  states for three-electron emission. The state-selective TPI cross sections have been obtained, although the formation mechanism of the TPI has not been specified in the current work. A detailed correlation analysis of the TPI will be made for investigating the presence of indirect processes.

#### ACKNOWLEDGMENTS

We are grateful to the Photon Factory staff for the stable operation of the storage ring. We also thank V.A. Kilin for providing us with results of his calculation. This work was performed under the approval of the Photon Factory Advisory Committee (Proposals Nos. 2004G210 and 2006G230).

- 
- [1] J. A. R. Samson, in *Encyclopedia of Physics*, edited by W. Mehlhorn (Springer-Verlag, Berlin, 1982), Vol. 31, p. 123.
- [2] J. C. Levin, D. W. Lindle, N. Keller, R. D. Miller, Y. Azuma, N. B. Mansour, H. G. Berry, and I. A. Sellin, *Phys. Rev. Lett.* **67**, 968 (1991).
- [3] U. Becker, R. Wehlitz, O. Hemmers, B. Langer, and A. Menzel, *Phys. Rev. Lett.* **63**, 1054 (1989).
- [4] T. A. Carlson, *Phys. Rev.* **156**, 142 (1967).
- [5] D. M. P. Holland, K. Codling, J. B. West, and G. V. Marr, *J. Phys. B* **12**, 2465 (1979).
- [6] R. J. Bartlett, P. J. Walsh, Z. X. He, Y. Chung, E.-M. Lee, and J. A. R. Samson, *Phys. Rev. A* **46**, 5574 (1992).
- [7] N. Saito and I. H. Suzuki, *Int. J. Mass Spectrom. Ion Process.* **115**, 157 (1992).
- [8] J. A. R. Samson, R. J. Bartlett, and Z. X. He, *Phys. Rev. A* **46**, 7277 (1992).
- [9] T. N. Chang and R. T. Poe, *Phys. Rev. A* **12**, 1432 (1975).
- [10] S. L. Carter and H. P. Kelly, *Phys. Rev. A* **16**, 1525 (1977).
- [11] V. A. Kilin, D. A. Lazarev, Dm A. Lazarev, M. Y. Amusia, K. H. Schartner, A. Ehresmann, and H. Schmoranzner, *J. Phys. B* **33**, 4989 (2000).
- [12] V. A. Kilin (private communication).
- [13] K. H. Schartner, G. Mentzel, B. Magel, B. Möbus, A. Ehresmann, F. Vollweiler, and H. Schmoranzner, *J. Phys. B* **26**, L445 (1993).
- [14] K. H. Schartner, P. Lenz, B. Möbus, H. Schmoranzner, and M. Wildberger, *Phys. Lett. A* **128**, 374 (1988).
- [15] U. Becker, *J. Electron Spectrosc. Relat. Phenom.* **75**, 23 (1995).
- [16] R. Wehlitz, F. Heiser, O. Hemmers, B. Langer, A. Menzel, and U. Becker, *Phys. Rev. Lett.* **67**, 3764 (1991).
- [17] J. H. D. Eland, O. Vieuxmaire, T. Kinugawa, P. Lablanquie, R. I. Hall, and F. Penent, *Phys. Rev. Lett.* **90**, 053003 (2003).
- [18] K. Ono, J. H. Oh, K. Horiba, M. Mizuguchi, M. Oshima, T. Kiyokura, F. Maeda, Y. Watanabe, A. Kakizaki, T. Kikuchi, A. Yagishita, and H. Kato, *Nucl. Instrum. Methods Phys. Res. A* **467–478**, 573 (2001).
- [19] E. Shigemasa, A. Toyoshima, Y. Yan, T. Hayaishi, K. Soejima, T. Kiyokura, and A. Yagishita, *J. Synchrotron Radiat.* **5**, 777 (1998).
- [20] Y. Hikosaka, T. Aoto, P. Lablanquie, F. Penent, E. Shigemasa, and K. Ito, *J. Phys. B* **39**, 3457 (2006).
- [21] Y. Hikosaka, T. Aoto, P. Lablanquie, F. Penent, E. Shigemasa, and K. Ito, *Phys. Rev. Lett.* **97**, 053003 (2006).
- [22] J. M. Bizau and F. J. Wuilleumier, *J. Electron Spectrosc. Relat. Phenom.* **71**, 205 (1995).
- [23] T. Schneider, P. L. Chocian, and J.-M. Rost, *Phys. Rev. Lett.* **89**, 073002 (2002).
- [24] P. Bolognesi, L. Avaldi, D. R. Cooper, M. Coreno, R. Camillon, and G. C. King, *J. Phys. B* **35**, 2927 (2002).
- [25] A. Kikas, S. J. Osborne, A. Ausmees, S. Svensson, O. P. Sairanen, and S. Aksela, *J. Electron Spectrosc. Relat. Phenom.* **77**, 241 (1996).
- [26] M. Kitajima, H. Yoshida, A. De Fanis, G. Prümper, U. Hergenhan, E. Kuk, T. Tanaka, K. Nakagawa, H. Tanaka, S. Fritzsche, I. P. Sazhina, N. M. Kabachnik, and K. Ueda, *J. Phys. B* **39**, 1299 (2006).
- [27] U. Becker and R. Wehlitz, *J. Electron Spectrosc. Relat. Phenom.* **67**, 341 (1994).
- [28] N. Scherer, B. Krässig, and V. Schmidt, *Phys. Essays* **13**, 458 (2000).
- [29] J. A. R. Samson and G. C. Angel, *Phys. Rev. Lett.* **61**, 1584 (1988).
- [30] J. B. Bluett, D. Lukic, and R. Wehlitz, *Phys. Rev. A* **69**, 042717 (2004).
- [31] A. E. Kramida, T. Bastin, E. Biemont, P.-D. Dumont, and H.-P. Garnir, *Eur. Phys. J. D* **7**, 525 (1999).
- [32] L. Avaldi, G. Dawber, N. Gulley, H. Rojas, G. C. King, R. Hall, M. Stuehec, and M. Zitnik, *J. Phys. B* **30**, 5197 (1997).